8-7-2020

Tonic TCR Signaling Inversely Regulates the Basal Metabolism of CD4

Ashley A Viehmann Milam

Juliet M Bartleson

Michael D Buck

Chih-Hao Chang

Alexey Sergushichev

See next page for additional authors

Authors

Ashley A Viehmann Milam, Juliet M Bartleson, Michael D Buck, Chih-Hao Chang, Alexey Sergushichev, David L Donermeyer, Wing Y Lam, Erika L Pearce, Maxim N Artyomov, and Paul M Allen

Tonic TCR Signaling Inversely Regulates the Basal Metabolism of CD4 $^{+}$ T Cells

Ashley A. Viehmann Milam, Juliet M. Bartleson, Michael D. Buck, Chih-Hao Chang, Alexey Sergushichev, David L. Donermeyer, Wing Y. Lam, Erika L. Pearce, Maxim N. Artyomov and Paul M. Allen

ImmunoHorizons 2020, 4 (8) 485-497
doi: https://doi.org/10.4049/immunohorizons.2000055
http://www.immunohorizons.org/content/4/8/485

ImmunoHorizons is an open access journal published by
The American Association of Immunologists, Inc.,
1451 Rockville Pike, Suite 650, Rockville, MD 20852

ISSN 2573-7732.

ImmunoHorizons

RESEARCH ARTICLE

Adaptive Immunity

Tonic TCR Signaling Inversely Regulates the Basal Metabolism of CD4$^+$ T Cells

Ashley A. Viehmann Milam,*[,1] Juliet M. Bartleson,*[,1] Michael D. Buck,[†,‡] Chih-Hao Chang,[§] Alexey Sergushichev,[¶] David L. Donermeyer,* Wing Y. Lam,[‖] Erika L. Pearce,[†] Maxim N. Artyomov,* and Paul M. Allen*

*Division of Immunobiology, Department of Pathology and Immunology, Washington University School of Medicine, St. Louis, MO 63110; [†]Max Planck Institute of Immunobiology and Epigenetics, Freiburg 79108, Germany; [‡]The Francis Crick Institute, London NW1 1AT, United Kingdom; [§]The Jackson Laboratory, Bar Harbor, ME 04609; [¶]ITMO University, St. Petersburg, Russia 197101; and [‖]Amgen Research, Amgen, Inc., South San Francisco, CA 94080

ABSTRACT

The contribution of self-peptide–MHC signaling in CD4$^+$ T cells to metabolic programming has not been definitively established. In this study, we employed LLO118 and LLO56, two TCRtg CD4$^+$ T cells that recognize the same *Listeria* epitope. We previously have shown that LLO56 T cells are highly self-reactive and respond poorly in a primary infection, whereas LLO118 cells, which are less self-reactive, respond well during primary infection. We performed metabolic profiling and found that naive LLO118 had a dramatically higher basal respiration rate, a higher maximal respiration rate, and a higher glycolytic rate relative to LLO56. The LLO118 cells also exhibited a greater uptake of 2-NBD–glucose, in vitro and in vivo. We extended the correlation of low self-reactivity (CD5^{lo}) with high basal metabolism using two other CD4$^+$ TCRtg cells with known differences in self-reactivity, AND and Marilyn. We hypothesized that the decreased metabolism resulting from a strong interaction with self was mediated through TCR signaling. We then used an inducible knock-in mouse expressing the Scn5a voltage-gated sodium channel. This channel, when expressed in peripheral T cells, enhanced basal TCR-mediated signaling, resulting in decreased respiration and glycolysis, supporting our hypothesis. Genes and metabolites analysis of LLO118 and LLO56 T cells revealed significant differences in their metabolic pathways, including the glycerol phosphate shuttle. Inhibition of this pathway reverts the metabolic state of the LLO118 cells to be more LLO56 like. Overall, these studies highlight the critical relationship between peripheral TCR–self-pMHC interaction, metabolism, and the immune response to infection. *ImmunoHorizons*, 2020, 4: 485–497.

Received for publication June 22, 2020. Accepted for publication July 23, 2020.

Address correspondence and reprint requests to: Dr. Paul M. Allen, Washington University School of Medicine, 660 South Euclid Avenue, Campus Box 8118, St. Louis, MO 63110. E-mail address: pallen@wustl.edu

ORCIDs: 0000-0002-9611-1199 (M.D.B.); 0000-0002-0139-7439 (C.-H.C.); 0000-0003-1159-7220 (A.S.); 0000-0002-1133-4212 (M.N.A.).

[1]A.A.V.M. and J.M.B. contributed equally.

The microarray data presented in this article have been submitted to the Gene Expression Omnibus (https://www.ncbi.nlm.nih.gov/geo/) under accession number GSE146069.

This work was supported by National Institutes of Health Grants AI138393 (to J.M.B.), CA034196 (to C.-H.C.), CA181125 (to E.L.P.), AI125618 (to M.N.A.), and AI139540 (to P.M.A.) and European Molecular Biology Organization Fellowship 1096-2018 (to M.D.B.).

A.A.V.M. and J.M.B. designed and performed experiments, analyzed data, and wrote the manuscript, M.D.B., C.-H.C., D.L.D., A.S., and W.Y.L. performed experiments, analyzed data, and generated figures, M.N.A. analyzed data, E.L.P. designed experiments, and P.M.A. designed experiments and wrote the manuscript.

Abbreviations used in this article: DN, double-negative; DP, double-positive; ECAR, extracellular acidification rate; FCCP, carbonyl cyanide-*4*-(trifluoromethoxy) phenylhydrazone; GAM, Genes and Metabolites; 2-NBDG, 2-(*N*-(7-nitrobenz-2-oxa-1,3-diazol-4-yl)amino)-2-deoxyglucose; OCR, oxygen consumption rate; OXPHOS, oxidative phosphorylation; SRC, spare respiratory capacity.

INTRODUCTION

Initial metabolic analyses of T cells focused on differences between resting and activated cells. These studies established that naive T cells mainly use oxidative phosphorylation (OXPHOS) to generate the relatively low bioenergetic needs required by their quiescent state, whereas activated T cells shift their metabolism from OXPHOS to aerobic glycolysis to support the anabolic reactions demanded by clonal expansion and effector differentiation (1, 2). However, metabolic networks influence T cell function beyond simply meeting the energy demands of the T cell. A multitude of signaling pathways essential for various T cell functions are closely interconnected with metabolic programming, either through shared signaling components or directly through metabolite regulation (3). In the last decade, complex roles for distinct metabolic programming in nearly every facet of the T cell response to Ag have been further elucidated, encompassing expansion, differentiation, effector function, and memory cell formation and maintenance (3). Conversely, although there has been some work interrogating the metabolic intricacies of naive, quiescent T cells, this remains a relatively underappreciated area of T cell biology.

The dampening of metabolic activity in quiescent T cells is an active process (4). Studies have unveiled a critical role for mTOR1 inhibitors (i.e., TSC1, PTEN, and LKB1) in the enforcement of a quiescent program in naive, peripheral T cells. These molecules have been shown to have distinct effects on the regulation of T cell homeostasis; interestingly, their deletion also uniquely modifies how T cells respond to stimulation (5–7). This highlights the possibility that metabolic networks may prime naive T cells to tune their eventual response to Ag, leading us to question whether there is metabolic heterogeneity within the naive $CD4^+$ T cell population.

Activation of $CD4^+$ T cells involves the integration of multiple variables: TCR signaling, costimulation, and cytokine instruction. All three of these activating components have been shown to affect the metabolism of $CD4^+$ T cells. In a naive state, cytokine signaling and TCR signaling, through tonic self-pMHC interactions, also occur. IL-7R signaling has been previously shown to affect naive T cell metabolism, but this was considered in an all-or-none manner in which no IL-7R signaling lead to the death of naive T cells because of an inability to meet their quiescent bioenergetic needs (8); therefore, we wanted to determine whether subtle differences in tonic TCR signaling could generate a metabolically heterogenous pool of naive $CD4^+$ T cells.

Peripheral TCR–self-pMHC interactions are distinct from thymic–self-pMHC interactions, as they do not induce the same signals required for positive selection. Instead, peripheral tonic TCR signaling involves low-level stimulation that does not propagate canonical activation pathways, but rather generates nuanced effects on the activation state of the T cell and gene expression levels (9, 10). There is a wide range of tonic signaling strengths in the naive polyclonal T cell population, as determined by Nur77 (11, 12) and CD5 (13) expression. This implies that interactions of an individual TCR with a specific self-pMHC ligand controls the level of tonic signaling on a cellular basis.

Several studies involving blockade of TCR–self-pMHC interactions, either with anti–MHC class II Abs or genetic deletion of MHC class II on APCs, have revealed the role tonic signaling plays in survival, homeostatic expansion, and Ag reactivity of $CD4^+$ T cells (14–24). Interestingly, tonic signaling has also been linked to metabolic activity in memory $CD4^+$ T cells. When deprived of class II interactions, memory T cells responded poorly and had indications of overall diminished metabolic activity relative to T cells that maintained TCR–self-pMHC interactions (14, 16, 19). The two primary indicators of tonic TCR signaling strength, CD5 and Nur77, have also been shown to act as regulators of T cell metabolism postactivation to alter Teff function in vivo (25–27).

To explore whether tonic TCR signaling could influence a naive T cell's metabolic programming, we employed LLO56 and LLO118, two TCRtg $CD4^+$ T cells that recognize the same *Listeria monocytogenes* epitope with the same affinity, and which have been previously characterized by our laboratory (22, 28, 29). In this study, we show that naive LLO118 cells, which have low-tonic signaling, exhibit heightened basal metabolic activity when compared with their high-tonic signaling counterparts, LLO56. Specifically, metabolic profiling of the cells revealed that naive LLO118 had a higher basal respiration rate, maximal respiration rate, and spare respiratory capacity (SRC) relative to LLO56. LLO118 cells also had a higher glycolytic rate and took up more 2-NBD–glucose than LLO56. Furthermore, the emergence of these differences in LLO TCRtg metabolism coincided with the onset of positive selection in the developing thymocytes, underlining the dependence of naive metabolic programming on TCR–self-pMHC interactions.

Therefore, we hypothesized there was an inverse relationship between the strength of tonic signaling and basal metabolic activity in naive $CD4^+$ T cells, which was mediated through TCR signaling. We first confirmed that the metabolic phenotype observed in our LLO TCRtg cells extended to other high and low-tonic signaling $CD4^+$ T cells by interrogating the basal metabolism of another set of TCRtg T cells, as well as assessing glucose uptake in polyclonal $CD4^+$ T cells. We then tested our hypothesis by using a Scn5a/CD4-cre mouse line, which we have previously demonstrated to have polyclonal $CD4^+$ T cells with more sensitive TCR proximal signaling in response to peripheral self-pMHC (28). The metabolic properties of Scn5a-expressing naive $CD4^+$ T cells were assessed, and we found that the increased sensitivity to self resulted in decreased basal and maximal respiration rates, supporting our hypothesis. Collectively, these data establish a direct link between tonic TCR signaling and basal metabolic activity in $CD4^+$ T cells.

MATERIALS AND METHODS

Mice

The LLO56 and LLO118 TCR–transgenic lines, specific for listeriolysin O (190–205) ($LLO_{190–205}$/I-A^b), have been previously described (22, 28, 29). These mice were maintained on a Rag1-knockout background with homozygous congenic marker expression (LLO118-Ly5.1; LLO56-Thy1.1). The H-Y–specific Marilyn

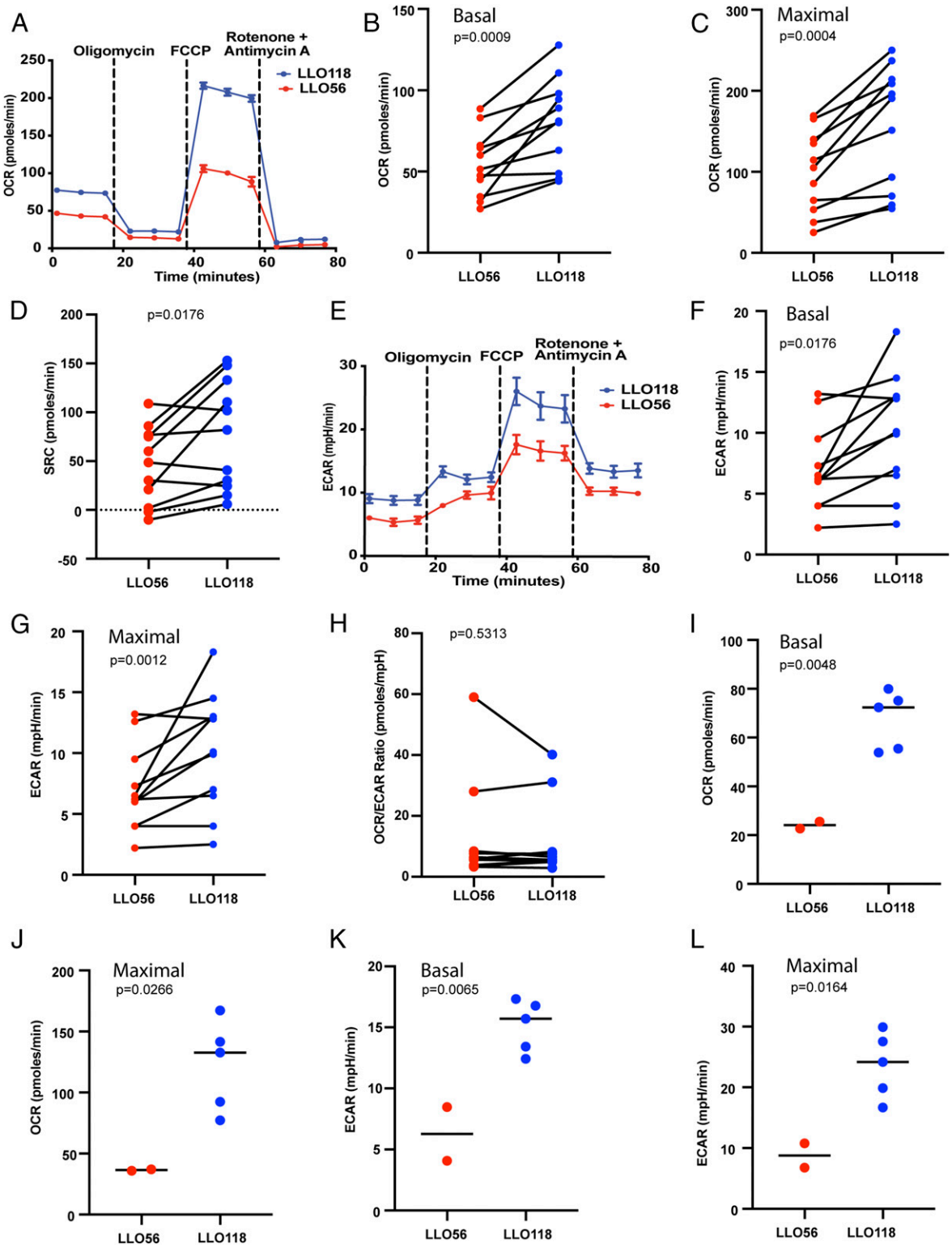

FIGURE 1. Naive LLO CD4+ T cells with low-tonic signaling exhibit a higher metabolism than those with high-tonic signaling.

(**A**) Enriched CD4+ T cells from spleens of LLO56 and LLO118 TCRtg mice were analyzed using a standard Seahorse protocol, with stepwise injections of oligomycin, FCCP, and rotenone plus antimycin A. A total of 2 to 3 × 10^5 cells per well were used, with the cell counts always matched between mice on individual runs, and a minimum of three wells per mouse were plated. The OCR, a readout of cellular respiration, was measured, and a representative OCR curve is shown. (**B**) Basal OCR, the first OCR data point collected, was plotted for LLO56 and LLO118 pairs from individual Seahorse runs (n = 10). Plot points represent averages of a minimum of three wells; p = 0.0009 by a paired t test. (**C**) Maximal OCR, **(Continued)**

https://doi.org/10.4049/immunohorizons.2000055

TCR–transgenic line was acquired from National Institute of Allergy and Infectious Diseases/Taconic, and the AND TCR–transgenic line (MCC-I-E^k–specific) and B6 mice were acquired from The Jackson Laboratory. Derivation of the polyclonal Scn5a-transgenic mouse (and its subsequent crossing to a CD4-Cre line) has also been previously described (28). All mice were bred and housed in a specific pathogen-free facility at Washington University, according to guidelines established by the Washington University Division of Comparative Medicine.

Seahorse analysis

Oxygen consumption rate (OCR) and extracellular acidification rate (ECAR) were measured using a 96-well XF extracellular flux analyzer (Seahorse Bioscience) and Extracellular Flux Assay Kit (XFe96; Agilent Seahorse). Assay setup has been previously described (30–33). Briefly, cells were plated in XF media supplemented with glucose (25 mM), L-glutamine (2 mM), and sodium pyruvate (1 mM). Measurements were taken at basal state, and after the stepwise addition of oligomycin (1 μM), carbonyl cyanide-4-(trifluoromethoxy) phenylhydrazone (FCCP) (1.5 μM), and rotenone (100 μM) plus antimycin A (1 μM). The mGPD2 specific inhibitor, iGP-1 (#5.30655.0001; Calbiochem/EMD Millipore) was dissolved in DMSO and added to the extracellular flux analyses at either 2.5 or 5.0 μM final concentration.

2-NBD–glucose uptake

To measure in vitro 2-NBD–glucose uptake in T cells, RBC lysis was performed on naive splenocytes. TCR-transgenic cells were further negatively bead enriched for $CD4^+$ T cells (Mouse $CD4^+$ T Cell Kit; Miltenyi Biotec), whereas polyclonal cells were not enriched. A total of 10^6 $CD4^+$ T cells or polyclonal splenocytes were then plated in duplicate in media (RPMI 1640 with 10% FBS and Life Technologies Glutamax) supplemented with 50 μg/ml 2-(*N*-(7-nitrobenz-2-oxa-1,3-diazol-4-yl)amino)-2-deoxyglucose (2-NBDG) (Cayman Chemical), for 20 min at 37°C. Cells were then washed twice in PBS and stained for FACS as described above. Only $CD4^+TCR\beta^+$ T cells were included in analysis. For in vivo uptake, 2-NBD–glucose was prepared at 200 mg/ml in PBS and injected i.p. at a dose of 1000 mg/kg. The mice were sacrificed after 15 min, the lymphoid organs harvested and analyzed as described above.

Flow cytometry

All samples were analyzed on BD FACSCanto II or BD LSRFortessa cytometers, and data were analyzed using FlowJo software (FlowJo). The following Abs/clones were used for cell analysis: CD3ε (clone 145-2C11, FITC; BioLegend; clone 145-2C11, allophycocyanin; BioLegend), CD4 (clone RM4.5, FITC; BioLegend; clone RM4.5, eFluor 450; eBioscience; clone RM4.5, PerCP-Cy5.5; eBioscience), CD5 (clone 53-7.3, FITC; BD Biosciences), CD8α (clone 53-6.7, allophycocyanin; BD Biosciences), CD45.1/Ly5.1 (clone A20, eFluor 450; eBioscience), CD90.1/Thy1.1 (clone OX-7, PE; BioLegend), and TCRβ (clone H57-597, PerCP-Cy5.5; BioLegend; clone H57-597, FITC; BD Biosciences).

Transcriptional profiling and genes and metabolites analysis

Transcriptional profiling of naive and D7 in vivo–activated LLO118 and LLO56 was performed using Affymetrix microarrays (Mouse Gene ST 1.0; Affymetrix) using standard Affymetric protocols. Naive LLO118 and LLO56 T cells were purified from the spleens of individual mice (n = 4) from each of the TCRtg lines using a Miltenyi $CD4^+$ Isolation Selection Kit (no. 130-104-454) following the manufacturer's instructions. For the D7 in vivo–activated T cell isolation, 10^4 of either LLO118 or LLO56 T cells were injected into a wild-type C57BL/6J mouse on day-1. On D0, they were infected with *L. monocytogenes* and the spleens from individual mice (LLO118 n = 4; LLO56 n = 3) were harvested on D7. The T cells were purified by FACS on a BD FACSAria by sorting on $CD4^+$ and the appropriate congenic marker (Thy1.1 for LLO118 and Ly5.1 for LLO56). A dump gate of CD8, CD11b, CD11c, CD19, NK1.1, and MHC class II was used. RNA was purified from 1.5 to 2 × 10^6 T cells using an RNeasy Mini Kit (no. 74104; Qiagen), the cDNA

the first OCR data point collected after the injection of FCCP, was plotted from pairs from individual Seahorse runs (n = 10). Plot points represent averages of a minimum of three wells; p = 0.0004 by a paired t test. (**D**) SRC was plotted from pairs from individual Seahorse runs (n = 10). SRC was calculated by subtracting the basal OCR from the maximal OCR; p = 0.0176 by a paired t test. (**E**) Enriched $CD4^+$ T cells from spleens of LLO56 and LLO118 TCRtg mice were run using a standard Seahorse protocol, as described in (A). The ECAR, a readout of cellular glycolysis, was measured, and a representative ECAR curve is shown. (**F**) Basal ECAR, the first ECAR data point collected, was plotted for LLO56 and LLO118 pairs from individual Seahorse runs (n = 10). Plot points represent averages of a minimum of three wells; p = 0.0176 by a paired t test. (**G**) Maximal ECAR, the first ECAR data point collected after the injection of FCCP, was plotted for LLO56 and LLO118 pairs from individual Seahorse runs (n = 10). Plot points represent averages of a minimum of three wells; p = 0.0012 by a paired t test. (**H**) To determine the relative reliance of a $CD4^+$ T cell population on cellular respiration versus cellular glycolysis, the ratio of OCR/ECAR was calculated by dividing the maximal OCR by the maximal ECAR for each pair of LLO56 and LLO118; p = 0.5313 by a paired t test. (**I**) Basal OCR of LLO56 and LLO118 T cells on D7 after in vivo activation by *L. monocytogenes* infection as described in (B). The values represent the average of a minimum of three individual wells from individual mice from two independent experiments; p = 0.0048 by an unpaired t test. (**J**) Maximal OCR of LLO56 and LLO118 T cells on D7 after in vivo activation by *Listeria* infection as described in (C). The values represent the average of a minimum of three individual wells from individual mice from two independent experiments; p = 0.0266 by an unpaired t test. (**K**) Basal ECAR of LLO56 and LLO118 T cells on D7 after in vivo activation by *Listeria* infection as described in (F). The values represent the average of a minimum of three individual wells from individual mice from two independent experiments; p = 0.0065 by an unpaired t test. (**L**) Maximal ECAR of LLO56 and LLO118 T cells on D7 after in vivo activation by *Listeria* infection as described in (G). The values represent the average of a minimum of three individual wells from individual mice from two independent experiments; p = 0.0164 by an unpaired t test.

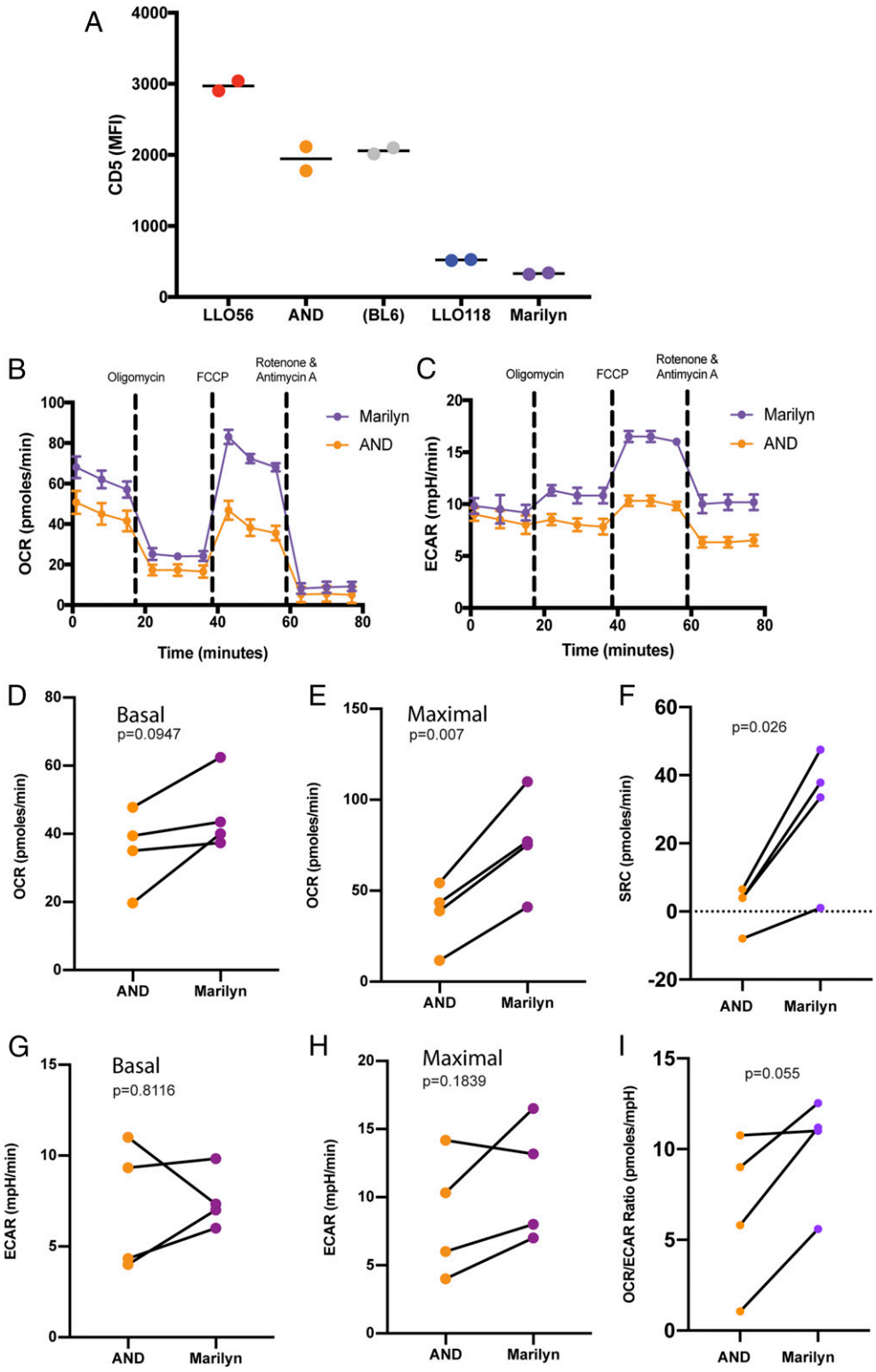

FIGURE 2. Use of a second pair of low- and high-tonic signaling TCRtg CD4+ T cells, Marilyn and AND, respectively, further confirms that low-tonic signaling correlates with increased basal metabolic activity.

(**A**) Mean CD5 levels are indicated for the four transgenic lines analyzed (LLO56, AND, LLO118, Marilyn), as well as a BL6 mouse (n = 2 mice each). (**B**) Enriched CD4+ T cells from spleens of Marilyn and AND TCRtg mice were analyzed using a standard Seahorse protocol, as described in Fig. 1. A representative OCR curve is shown. (**C**) Enriched CD4+ T cells from spleens of Marilyn and AND TCRtg mice were run using a standard Seahorse protocol. A representative ECAR curve is shown. (**D**) Basal OCR, the first OCR data point collected, was plotted for Marilyn and AND **(Continued)**

https://doi.org/10.4049/immunohorizons.2000055

prepared using a NuGen Pico SL Kit, and 5.5 μg of cDNA was hybridized to the microarrays using standard Affymetric protocols. All data were normalized using RMA in Arraystar 12. Microarray data have been deposited in the Gene Expression Omnibus (https://www.ncbi.nlm.nih.gov/geo/) under accession number GSE146069. Genes and metabolites analysis was performed comparing the naive LLO118 and LLO56 T cells and D7 in vivo–activated LLO118 and LLO56 T cells using Genes and Metabolities (GAM) (https://artyomovlab.wustl.edu/shiny/gam/) on an atom-based network (34, 35).

Bacterial infections

The *L. monocytogenes* strain 1043S used in this study was generously provided by D. Portnoy (University of California, Berkeley, CA), and *L. monocytogenes* infections of LLO56 and LLO118 mice were performed as previously described (28).

Statistical analysis

Prism (versions 7 and 8) software for Mac OS X was used for all statistical analysis. Statistical significance was determined using either a paired *t* test (for Seahorse runs), an unpaired *t* test, or an ANOVA test, and a p value <0.05 was designated as the criterion for significance.

RESULTS

In naive mice, CD4+ T cells with lower tonic signaling have higher rates of respiration and glycolysis than CD4+ T cells with higher tonic signaling

To compare the basal metabolic profiles of LLO56 and LLO118, splenocytes of naive, age-and sex-matched matched mice were enriched for CD4+ T cells, and Seahorse platform analysis was performed on the enriched populations. The respiratory rate of LLO118 cells was higher than that of LLO56 cells, as evidenced by the higher OCR of these cells (Fig. 1A). Specifically, baseline respiration was higher in naive LLO118 CD4+ T cells than in naive LLO56 cells, as was maximal respiration, reached after addition of the uncoupling reagent FCCP (Fig. 1B, 1C). SRC, which has been defined as a cell's energy reserve capable of fueling cellular function above and beyond basic energy needs, was also higher in LLO118 than in LLO56 (36) (Fig. 1D). Likewise, glycolytic function was greater in LLO118 than in LLO56, as evidenced by the higher basal ECAR and the higher maximal ECAR of LLO118 cells (Fig. 1E–G). Interestingly, we found no difference in the ratio of OCR to ECAR in LLO56 and LLO118 cells, indicating that they have similar relative reliance on respiration and glycolysis for meeting energy needs (Fig. 1H). The same metabolic differences between LLO118 and LLO56 were observed when the LLO T cells were activated in vivo with *Listeria* and harvested on d7 postinfection, during which LLO118 T cells had a greater OCR and ECAR than LLO56 cells (Fig. 1I–L). Overall, these findings indicate that the less self-reactive LLO118 CD4+ T cell is more metabolically active in its naive state than the more self-reactive LLO56 cell.

To determine whether the inverse correlation between tonic signaling and basal metabolism was specific to the LLO system or generalizable to other systems, we also interrogated the basal metabolism of another set of CD4+ T cell transgenics, AND, and Marilyn. AND recognizes Moth cytochrome C (MCC)/I-E^k (37), whereas Marilyn recognizes the male Y Ag/I-A^b (38). Mandl et al. (13) examined a panel of TCRtg lines, including AND and Marilyn, for their level of tonic signaling. Similar to LLO56, AND has high-tonic signaling and thus expresses high levels of CD5; like LLO118, Marilyn has lower tonic signaling and expresses lower levels of CD5 (Fig. 2A). Mirroring our findings in the LLO system, the $CD5^{lo}$ Marilyn T cell had higher maximal respiration relative to AND (Fig. 2B, 2E) and SRC (Fig. 2F); however, there was not a significant difference in the basal metabolism (Fig. 2D). Maximal glycolytic rates trended to be higher in Marilyn than in AND, but did not reach a level of significance (Fig. 2C, 2H). The ratio of OCR to ECAR in AND and Marilyn T cells did not reach a level of significance, indicating that they have similar relative reliance on respiration and glycolysis for meeting energy needs (Fig. 2I). Collectively, these findings in the AND/Marilyn TCR systems further supported our observation that cells with lower tonic signaling have a higher metabolic capacity in their naive state.

Increased 2-NBD–glucose uptake correlates with the higher basal metabolism in low-tonic signaling cells

Because we observed enhanced glycolysis in LLO118 compared with LLO56, we also sought to determine if glucose uptake was enhanced in these cells. To test this, we measured in vitro uptake of 2-NBDG, a nonmetabolizable glucose analogue, in LLO56 and LLO118 T cells (39). Complementing our observation of higher glycolysis in LLO118 cells, 2-NBDG uptake was approximately twice as high in LLO118 cells as it was in LLO56 cells (Fig. 3A, 3B). 2-NBDG uptake was also measured in vivo following i.p. injection, and we observed higher 2-NBDG uptake in LLO118 cells, relative to LLO56 cells (Fig. 3C). Similarly, 2NBDG uptake was also higher in Marilyn cells relative to AND in vitro (Fig. 3D, 3E). We were further able to

pairs from individual Seahorse runs (n = 4). Plot points represent averages of a minimum of three wells; p = 0.0947 by a paired *t* test. (**E**) Maximal OCR, the first OCR data point collected after the injection of FCCP, was plotted from Marilyn and AND pairs from individual Seahorse runs (n = 4). Plot points represent averages of a minimum of three wells; p = 0.007 by a paired *t* test. (**F**) SRC was plotted from pairs of individual Seahorse runs. SRC was calculated by subtracting the basal OCR from the maximal OCR. (**G**) Basal ECAR, the first ECAR data point collected, was plotted for Marilyn and AND pairs from individual Seahorse runs (n = 4). Plot points represent averages of a minimum of three wells. (**H**) Maximal ECAR, the first ECAR data point collected after the injection of FCCP, was plotted for Marilyn and AND pairs from individual Seahorse runs (n = 4). Plot points represent averages of a minimum of three wells. (**I**) The ratio of OCR/ECAR was calculated by dividing the maximal OCR by the maximal ECAR for each pair and the plot points represent averages of a minimum of three wells.

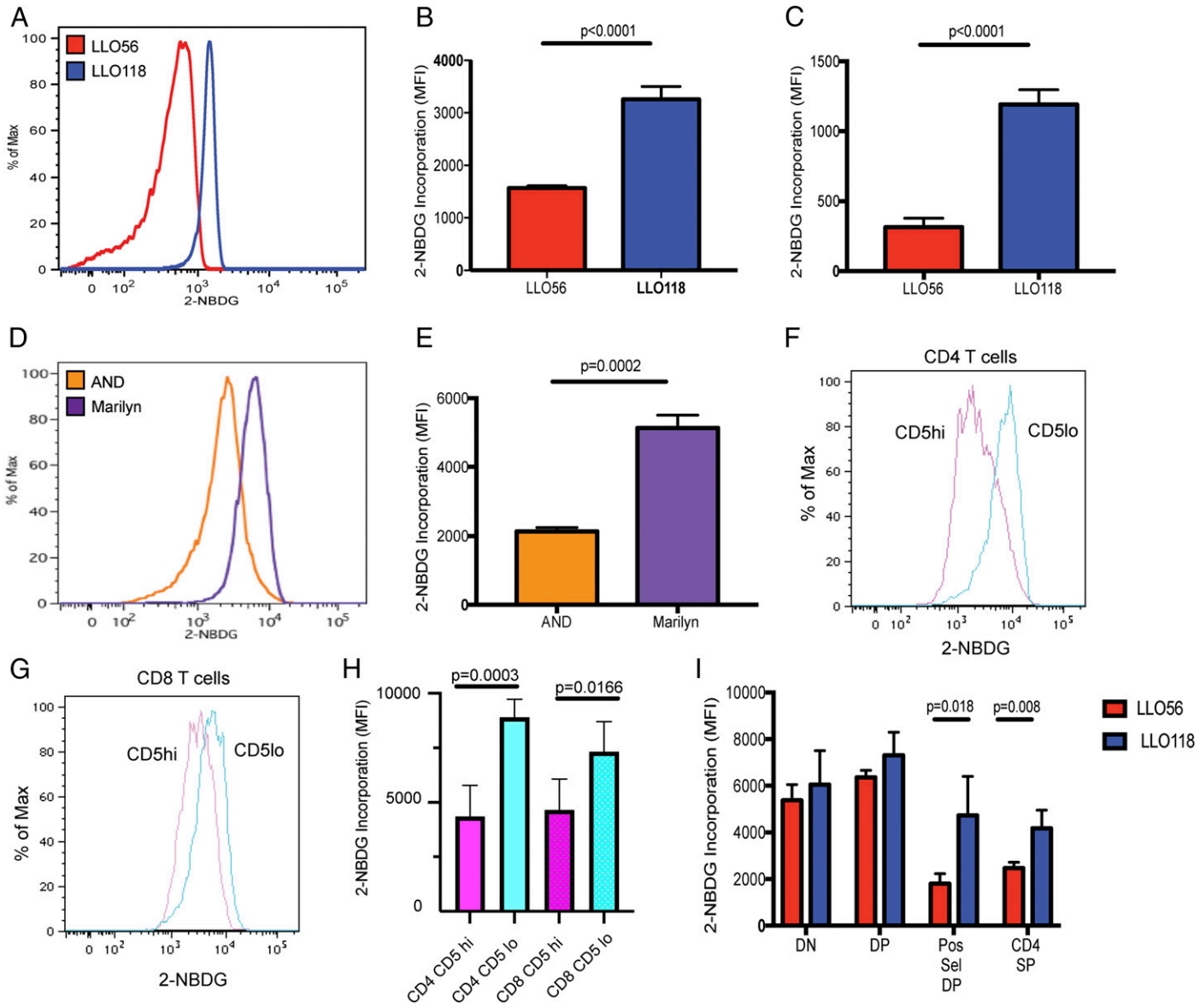

FIGURE 3. 2-NBD–Glucose uptake analysis reveals metabolic differences between low- and high-tonic signaling CD4$^+$ T cells can be extended to the polyclonal population, and this difference emerges after initial TCR–self-pMHC interactions in the thymus.

(**A**) 2-NBDG uptake in naive splenocytes from either LLO56 (n = 3) or LLO118 (n = 4) mice was measured by FACS after a 20-min in vitro incubation. Live/dead gating was used on single-cell suspensions, followed by doublet discrimination. Cells were then gated on the CD3$^+$CD4$^+$ population, and a representative histogram is shown. (**B**) Quantified in vitro uptake is shown, and data are representative of three independent experiments. (**C**) In vivo 2-NBDG uptake was measured by FACS 15 min after an IP injection of 2-NBDG in LLO56 (n = 4) and LLO118 (n = 4) mice. Live/dead gating was used on single-cell suspensions, followed by doublet discrimination. Cells were then gated on the CD3$^+$CD4$^+$ population, and quantified uptake is shown. Data are representative of three independent experiments. (**D**) 2-NBDG uptake in naive splenocytes from either AND (n = 3) or Marilyn (n = 3) mice was measured by FACS after a 20-min in vitro incubation. Live/dead gating was used on single-cell suspensions, followed by doublet discrimination. Cells were then gated on the CD3$^+$CD4$^+$ population, and a representative histogram is shown. (**E**) Quantified in vitro uptake is shown, and data are representative of three independent experiments. (**F**) 2-NBDG uptake in naive splenocytes from a total of five individual C57BL/6J mice in two separate experiments, was measured by FACS after a 20-min in vitro incubation. Live/dead gating was used on single-cell suspensions, followed by doublet discrimination. Cells were then gated on the CD3$^+$CD4$^+$ population, and then further gated on CD5 expression (highest 10% and lowest 10%). A representative is shown. (**G**) 2-NBDG uptake in naive splenocytes from a total of five individual C57BL/6J mice in two separate experiments, was measured by FACS after a 20-min in vitro incubation. Live/dead gating was used on single-cell suspensions, followed by doublet discrimination. Cells were then gated on the CD3$^+$CD8$^+$ population, and then further gated on CD5 expression (highest 10% and lowest 10%). A representative is shown. (**H**) Quantified uptake is shown of 2-NBDG in polyclonal CD4$^+$ (n = 5) and CD8$^+$ (n = 5) T cells gated on **(Continued)**

https://doi.org/10.4049/immunohorizons.2000055

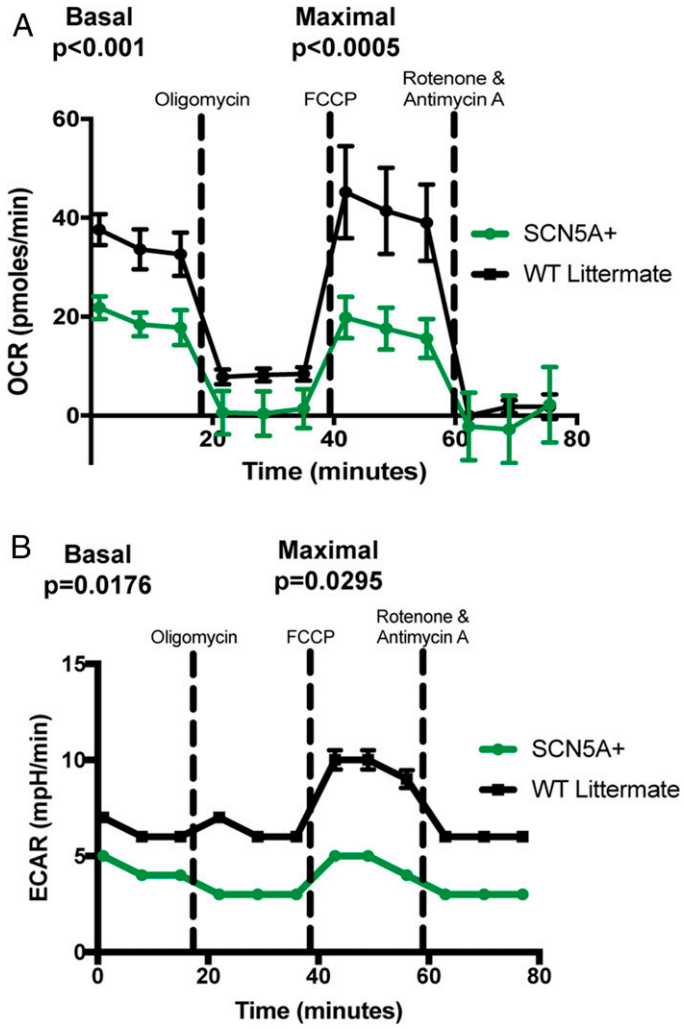

FIGURE 4. Increasing TCR signaling results in correspondingly lower respiration and glycolysis rates in naive CD4+ T cells.

(**A**) Enriched CD4+ T cells from spleens of Scn5+CD4−cre+ mice and Scn5+CD4−cre− mice were analyzed using a standard Seahorse protocol as described in Fig. 1. Shown is the OCR of three combined experiments, with the points representing the mean ± SEM. The *p* values are shown for the basal (time 0′) and maximal (time 42′) values. (**B**) Enriched CD4+ T cells from spleens of from Scn5+CD4−cre+ mice and Scn5+CD4−cre− paired mice were run using a standard Seahorse protocol as described in Fig. 1. Shown is the ECAR of three combined experiments, with the points representing the mean ± SEM. The *p* values are shown for the basal (time 0′) and maximal (time 42′) values.

extend this finding into polyclonal T cells, in which we observed an inverse correlation between CD5 levels and 2-NBDG uptake (Fig. 3F–H). In C57BL/6J mice, peripheral CD4+ T cells with the lowest 10% of CD5 expression in vitro took up significantly more 2-NBDG than peripheral CD4+ T cells with the highest 10% of CD5 expression (Fig. 3F, 3H). A similar distinction in 2-NBDG uptake between CD5lo and CD5hi was observed for CD8+ T cells (Fig. 3G, 3H). It should be noted that the CD5lo and CD5hi populations are not completely comprised of native cells, but normal mice from our mouse colony have very low levels of activated T cells. Thus, the majority of the T cells we examined were naive. These findings show an inverse correlation between strength of TCR–self-pMHC interactions and metabolism existed for both CD4+ and CD8+ T cells.

To determine if we could identify the divergence of glucose uptake in the developmental timeline of LLO56 and LLO118, we also examined different populations of thymocytes in vitro. We found that in developing thymocytes, CD4−CD8− double-negative (DN) thymocytes from LLO56 and LLO118 take up similar amounts of 2-NBDG in vitro, as do CD4+CD8+ double-positive (DP) thymocytes. However, starting in positively selected DP (in this study, defined as CD4+CD8+ thymocytes expressing very high levels of TCRβ and CD5) and CD4 single-positive, 2-NBDG uptake in LLO56 decreases much more than the uptake of LLO118 (Fig. 3I). As this observed change coincided with the onset of positive selection (and therefore TCR signaling), it supports our hypothesis that increased self-pMHC–TCR interaction in a CD4+ T cell predisposes that cell to lower basal metabolism.

Peripheral CD4+ T cells with increased sensitivity to self-pMHC have decreased basal metabolism

To further elucidate the relationship between self-reactivity and metabolism in polyclonal CD4+ T cells, we sought a method that would allow us to genetically control metabolism. To this end, we employed a knock-in mouse line with inducible expression of Scn5a (sodium channel protein type five subunit α) (28). Scn5a is the pore-forming component of a voltage-gated sodium channel typically expressed in cardiac myocytes. We previously reported that when Scn5a is ectopically expressed in DP thymocytes, they are endowed with enhanced signaling to weak self-pMHC ligands during positive selection. Scn5a expression in CD4+ T cell hybrids equips them with increased sensitivity to self-pMHC, to the level that they are capable of responding to their positive-selecting peptide (40). Recently, we demonstrated that expression of Scn5a in peripheral CD4+ T cells (using Scn5a+CD4−Cre+ mice) resulted in increased proximal TCR signaling and increased peripheral CD5 expression and this expression of Scn5a in the LLO118 T cells led to an impaired in vivo response to *L. monocytogenes*

CD5hi and CD5lo populations. (**I**) in vitro 2-NBDG uptake in naive thymocytes from either LLO56 (n = 4) or LLO118 (n = 4) mice was measured by FACS after a 20-min incubation. Live/dead gating was used on single-cell suspensions, followed by doublet discrimination. Cells were then gated based on CD4 and CD8 expression into DP (CD4+CD8+), DN (CD4−CD8−), and single-positive (SP; CD4+CD8−) populations. Within the DP population, another gate was drawn on TCRβ++/CD5++ cells to interrogate DP cells initiating the process of positive selection. The 2-NBDG uptake of each population is shown, and data are representative of three independent experiments.

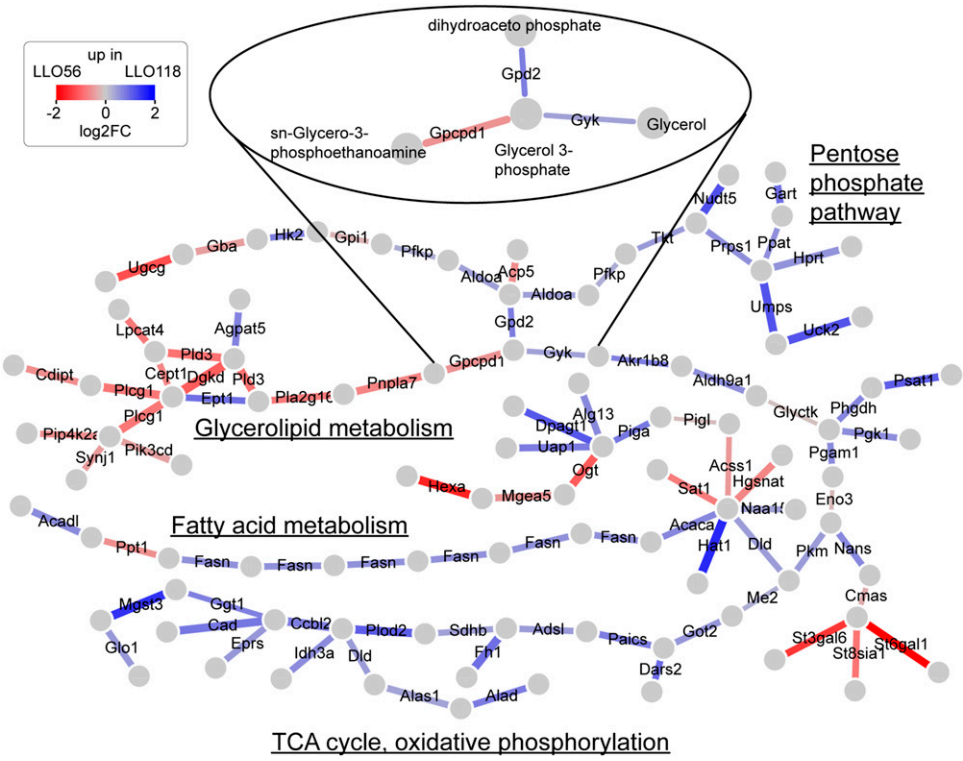

FIGURE 5. Metabolic pathway differences between LLO118 and LLO56 and identification of mGPD2 as a candidate gene.
Microarray data for LLO118 and LLO56 T cells activated in vivo by *L. monocytogenes* infection were analyzed on D7 post infection for metabolic pathway differences using the GAM program, revealing significant differences between the two T cells. The pathways upregulated in LLO118 are shown in blue, and those in LLO56 shown in red, with the intensity of the lines corresponding to the level of transcription. The enzymes involved in each step of the pathways are shown. For clarity, the substrates and products have been omitted. The inset highlights a key branch point between LLO118 and LLO56 T cells, highlighting mGPD2 as a candidate gene involved for the observed metabolic differences.

infection (28). To directly test the impact of increased sensitivity to self-pMHC on metabolism, we used Seahorse platform analysis to compare Scn5a$^+$CD4$^-$Cre$^+$ mice to Scn5a$^+$CD4$^-$Cre–negative littermates. Mirroring the differences we observed in LLO56 and LLO118 basal metabolism, we found that increasing self-sensitivity in Scn5a$^+$CD4$^-$Cre$^+$ mice led to a compensatory decrease in basal respiration (Fig. 4A), maximal respiration (Fig. 4A), and basal ECAR (Fig. 4B) and maximal ECAR (Fig. 4B). These data indicate that increasing TCR signaling sensitivity in naive CD4$^+$ T cells results in a compensatory decrease in metabolism.

Identification of metabolic pathway differences between the LLO T cells in their activated states

To gain unbiased insight into differences between LLO118 and LLO56 CD4$^+$ T cells, we performed transcriptional profiling of naive LLO118 and LLO56 T cells and those isolated at D7 postinfection. The naive cells had few transcriptional differences, with no obvious candidates to explain their distinct characteristics. We then analyzed the D7 data in the context of metabolic networks by using GAM analysis (34). Using this innovative approach, we found coordinated changes in a number of metabolic pathways (Fig. 5). Overall, LLO118 cells appeared to be metabolically much more active than LLO56 cells, consistent with our Seahorse analysis (Fig. 1). We found a metabolic bifurcation point that discriminated between LLO118-like metabolism and LLO56-like metabolism, centered at glycerol 3-phosphate (Fig. 5, inset). In LLO118 T cells, this metabolite can be directed toward the glycerol phosphate shuttle via the action of mitochondrial glycerol phosphate dehydrogenase (mGpd2). In LLO56 T cells, glycerol 3-phosphate is directed toward glycerolipid metabolism via the enzyme glycerophosphocholine phosphodiesterase 1 (Gpcpd1). The glycerol phosphate shuttle is a secondary mechanism that allows NADH generated in the cytosol by glycolysis to contribute to OXPHOS in the mitochondria, and thereby sustain ATP production (reviewed in Ref. 41). The rate-limiting enzyme for the glycerol phosphate shuttle is mGPD2. mGPD2 is a mitochondrial flavin-linked respiratory chain dehydrogenase that oxidizes glycerol-3-phosphate to dihydroxyacetone phosphate with concurrent reduction of FAD to $FADH_2$ and transfer of electrons to CoQ (Fig. 5 inset) (41). Recently, the glycerol phosphate shuttle has been shown to regulate macrophage inflammatory responses (42) and promote skeletal muscle regeneration (43), supporting the concept that it could be involved in the observed metabolic differences between LLO118 and LLO56 T cells.

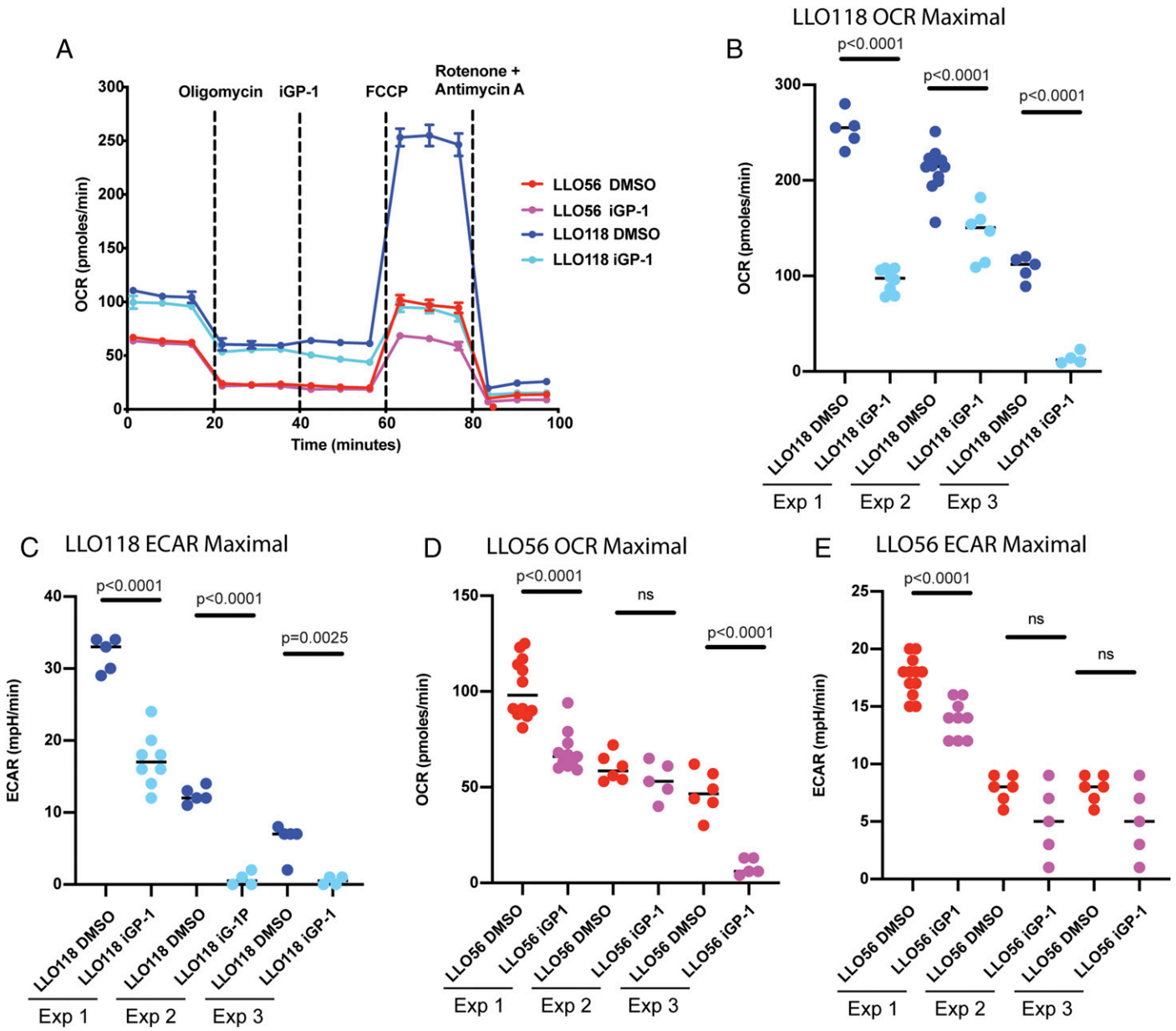

FIGURE 6. Inhibition of the glycerol phosphate shuttle reduces the metabolism of LLO118 cells.

(**A**) Metabolic analysis using the Seahorse platform was performed on LLO118 and LLO56 T cells. The specific inhibitor of glycerol 3 phosphate dehydrogenase (iGP-1, dissolved in DMSO), a key enzyme in the glycerol phosphate shuttle, was added at a final concentration of either 2.5 or 5 μM. A representative OCR curve is shown (n = 3). (**B**) Maximum OCR of LLO118 T cells from three individual experiments treated with iGP-1. The values represent individual wells with the mean value shown. The data from (A) are included in this graph. An unpaired t test was performed for each individual experiment. (**C**) Maximum ECAR of LLO118 T cells from three individual experiments treated with iGP-1. The values represent individual wells with the mean value shown. An unpaired t test was performed for each individual experiment. (**D**) Maximum OCR of LLO56 T cells from three individual experiments treated with iGP-1. The values represent individual wells with the mean value shown. The data from (A) are included in this graph. An unpaired t test was performed for each individual experiment. (**E**) Maximum ECAR of LLO56 T cells from three individual experiments treated with iGP-1. The values represent individual wells with the mean value shown. An unpaired t test was performed for each individual experiment.

Enhanced glycerol phosphate shuttle function contributes to basal metabolism of LLO118

To obtain evidence in support of the glycerol phosphate shuttle in the enhanced metabolism of LLO118 T cells, we targeted the mGpd2 enzyme, using an available specific inhibitor, iGP-1 (44). iGP-1 specifically inhibits the enzymatic activity of mitochondrial GPD2 (mGPD2), but not the cytosolic GPD2 isoform (44). iGP-1 is cell permeable but not bioavailable in vivo. Treatment of the LLO118 T cells in vitro with the iGP-1 significantly reduced their metabolic OCR and ECAR (Fig. 6A–C). Treatment of the LLO56 T cells with iGP-1 had a significant but weaker effect on their metabolism (Fig. 6A, 6D, 6E). This finding provides support for the involvement of the glycerol phosphate shuttle in the increased metabolism of the LLO118 T cells.

DISCUSSION

Interactions between a T cell through its TCR and self-pMHC on APCs are critical for the development and maintenance of an adaptive immune system. The role of self-pMHC in positive selection of T cells in the thymus is well established (reviewed in Ref. 45). TCR–self-pMHC interactions in the periphery are important for survival of T cells and initiation of activation. In this present study, we extended the role of these self-pMHC complexes to being involved in setting the basal metabolism of naive T cells. In a polyclonal T cell repertoire, there is a continuum of strengths of interactions with self-pMHC, and we have shown that there is an inverse relationship between the strength of these interactions and basal metabolism. Thus, T cells with the weaker interactions have a higher basal metabolism, and conversely those with stronger interactions have lower basal metabolisms. We propose that the reason for this tuning of the basal metabolism is that it represents a homeostatic balance between activation and autoimmunity, and permits the full T cell repertoire to participate in immune responses. There is emerging evidence that there are functional differences in $CD4^+$ T cells with different strengths of self-pMHC reactivity, which would support the notion that tuning of self-reactivity, metabolism, and T cell function allows the full repertoire to be involved in some aspect of an immune response (12, 13, 28, 29, 46). Other factors besides the level of self-reactivity of T cells can also be involve in regulating metabolism, such as the level of cytokine receptors. Anergic self-reactive T cells and T regulatory cells have been shown to have altered metabolism comparted to naive cells (47), but the development of both of these populations is still influenced by the strength of the TCR–self-pMHC interactions.

Through the analysis of transcriptional data by the GAM program (34), we identified the glycerol phosphate shuttle as one potential key metabolic pathway difference between T cells with high and low basal metabolisms. Thus, cells with higher basal metabolism require an increased glycerol phosphate shuttle function to provide NADH generated in the cytosol by glycolysis to contribute to OXPHOS in the mitochondria. Flavell and colleagues (48) have recently shown that the malate aspartate shuttle, another mechanism through which cytoplasmic NADH is shuttled to the mitochondria, was important in T cell differentiation. The malate aspartate shuttle was necessary for the proliferation of Th cells, whereas, succinate dehydrogenase subsequently antagonized differentiation and enforced terminal effector function. We have identified the enzyme mitochondrial glycerol phosphate dehydrogenase (mGPD2) as a potential key enzyme in the enhanced metabolism of T cells with weak self-pMHC interactions. mGPD2 has been recently shown by Horng and colleagues (42) to be a key regulator of glucose-oxidation in LPS-stimulated macrophages in the optimal control of inflammatory gene induction and suppression.

In these studies, we provide evidence of an inverse correlation between the level of self-reactivity and the metabolism of a T cell. There are some limitations from our experiments. It is currently very difficult to enhance tonic signaling in T cells. We have developed the $Scn5a^+$ model system, which does show an increase in the tonic signaling. We still do not know how the $Scn5a^+$ voltage-gated sodium channel is enhancing tonic signaling, and how it relates to the pathways normally involved in tonic signaling. We found increased uptake of the glucose analogue 2-NBD–glucose in cells with low-tonic signaling. Future studies of glucose metabolism in naive $CD4^+$ T cells is difficult with current techniques because naive T cells have a low uptake of labeled compounds needed to trace metabolic pathways and products (49). A recent promising report using a pulsed stable isotope labeling by amino acids in cell culture approach, showed that naive T cells have a large number of stalled ribosomes, which can rapidly respond upon T cell activation (50). They did not examine if naive T cells with high- and low-tonic signaling had differences in the number of stalled ribosomes in this initial report. The implication of mGPD2 in the enhanced metabolism between the LLO56 and LLO118 cells was based on the GAM analysis and use of the iGP-1 inhibitor. Many in vitro metabolic inhibitors have shown off-target effects. Clearly definitive genetic studies will have to be performed to establish the role of this pathway in basal metabolism, with the caveat of redundant metabolic pathways complicating the interpretation. Because mGPD2 is expressed in multiple immune cell types, a conditional knockout allele and a T cell–specific cre-deleter mouse should address this issue. Another area of future investigation will be to establish how signaling through the TCR via self-pMHC controls basal metabolism. Roose and colleagues (46) have made the important finding that tonic mTORC1 signals in naive $CD4^+$ T cells influence T cell fate decisions and that the Ras exchange factor Rasgrp1 is necessary to generate tonic mTORC1 signals. The well-established involvement of TORC1 in controlling cellular metabolism thus provides a potential mechanism by which the strength of TCR–self-pMHC interactions inversely regulate basal metabolism. Overall, our findings reveal an inverse relationship between the strength of tonic signaling in naive $CD4^+$ T cells and their basal metabolism, with important implications for T cell activation, differentiation, and function.

https://doi.org/10.4049/immunohorizons.2000055

DISCLOSURES

The authors have no financial conflicts of interest.

REFERENCES

1. Fox, C. J., P. S. Hammerman, and C. B. Thompson. 2005. Fuel feeds function: energy metabolism and the T-cell response. *Nat. Rev. Immunol.* 5: 844–852.
2. Jones, R. G., and C. B. Thompson. 2007. Revving the engine: signal transduction fuels T cell activation. *Immunity* 27: 173–178.
3. Geltink, R. I. K., R. L. Kyle, and E. L. Pearce. 2018. Unraveling the complex interplay between T cell metabolism and function. *Annu. Rev. Immunol.* 36: 461–488.
4. Chapman, N. M., M. R. Boothby, and H. Chi. 2020. Metabolic coordination of T cell quiescence and activation. *Nat. Rev. Immunol.* 20: 55–70.
5. Yang, K., G. Neale, D. R. Green, W. He, and H. Chi. 2011. The tumor suppressor Tsc1 enforces quiescence of naive T cells to promote immune homeostasis and function. *Nat. Immunol.* 12: 888–897.
6. Liu, X., J. L. Karnell, B. Yin, R. Zhang, J. Zhang, P. Li, Y. Choi, J. S. Maltzman, W. S. Pear, C. H. Bassing, and L. A. Turka. 2010. Distinct roles for PTEN in prevention of T cell lymphoma and autoimmunity in mice. *J. Clin. Invest.* 120: 2497–2507.
7. MacIver, N. J., J. Blagih, D. C. Saucillo, L. Tonelli, T. Griss, J. C. Rathmell, and R. G. Jones. 2011. The liver kinase B1 is a central regulator of T cell development, activation, and metabolism. *J. Immunol.* 187: 4187–4198.
8. Rathmell, J. C., E. A. Farkash, W. Gao, and C. B. Thompson. 2001. IL-7 enhances the survival and maintains the size of naive T cells. *J. Immunol.* 167: 6869–6876.
9. Guichard, V., N. Bonilla, A. Durand, A. Audemard-Verger, T. Guilbert, B. Martin, B. Lucas, and C. Auffray. 2017. Calcium-mediated shaping of naive CD4 T-cell phenotype and function. *eLife* 6: e27215.
10. Myers, D. R., J. Zikherman, and J. P. Roose. 2017. Tonic signals: why do lymphocytes bother? *Trends Immunol.* 38: 844–857.
11. Ashouri, J. F., and A. Weiss. 2017. Endogenous Nur77 is a specific indicator of antigen receptor signaling in human T and B cells. *J. Immunol.* 198: 657–668.
12. Zinzow-Kramer, W. M., A. Weiss, and B. B. Au-Yeung. 2019. Adaptation by naïve CD4+ T cells to self-antigen-dependent TCR signaling induces functional heterogeneity and tolerance. *Proc. Natl. Acad. Sci. USA* 116: 15160–15169.
13. Mandl, J. N., J. P. Monteiro, N. Vrisekoop, and R. N. Germain. 2013. T cell-positive selection uses self-ligand binding strength to optimize repertoire recognition of foreign antigens. *Immunity* 38: 263–274.
14. Bourgeois, C., G. Kassiotis, and B. Stockinger. 2005. A major role for memory CD4 T cells in the control of lymphopenia-induced proliferation of naive CD4 T cells. *J. Immunol.* 174: 5316–5323.
15. Brocker, T. 1997. Survival of mature CD4 T lymphocytes is dependent on major histocompatibility complex class II-expressing dendritic cells. *J. Exp. Med.* 186: 1223–1232.
16. De Riva, A., C. Bourgeois, G. Kassiotis, and B. Stockinger. 2007. Noncognate interaction with MHC class II molecules is essential for maintenance of T cell metabolism to establish optimal memory CD4 T cell function. *J. Immunol.* 178: 5488–5495.
17. Hochweller, K., G. H. Wabnitz, Y. Samstag, J. Suffner, G. J. Hämmerling, and N. Garbi. 2010. Dendritic cells control T cell tonic signaling required for responsiveness to foreign antigen. *Proc. Natl. Acad. Sci. USA* 107: 5931–5936.
18. Jameson, S. C. 2002. Maintaining the norm: T-cell homeostasis. *Nat. Rev. Immunol.* 2: 547–556.
19. Kassiotis, G., S. Garcia, E. Simpson, and B. Stockinger. 2002. Impairment of immunological memory in the absence of MHC despite survival of memory T cells. *Nat. Immunol.* 3: 244–250.
20. Martin, B., C. Bécourt, B. Bienvenu, and B. Lucas. 2006. Self-recognition is crucial for maintaining the peripheral CD4+ T-cell pool in a nonlymphopenic environment. *Blood* 108: 270–277.
21. Martin, B., C. Bourgeois, N. Dautigny, and B. Lucas. 2003. On the role of MHC class II molecules in the survival and lymphopenia-induced proliferation of peripheral CD4+ T cells. *Proc. Natl. Acad. Sci. USA* 100: 6021–6026.
22. Persaud, S. P., C. R. Parker, W. L. Lo, K. S. Weber, and P. M. Allen. 2014. Intrinsic CD4+ T cell sensitivity and response to a pathogen are set and sustained by avidity for thymic and peripheral complexes of self peptide and MHC. *Nat. Immunol.* 15: 266–274.
23. Stefanová, I., J. R. Dorfman, and R. N. Germain. 2002. Self-recognition promotes the foreign antigen sensitivity of naive T lymphocytes. *Nature* 420: 429–434.
24. Wülfing, C., C. Sumen, M. D. Sjaastad, L. C. Wu, M. L. Dustin, and M. M. Davis. 2002. Costimulation and endogenous MHC ligands contribute to T cell recognition. [Published erratum appears in 2002 *Nat. Immunol.* 3: 305.] *Nat. Immunol.* 3: 42–47.
25. Henderson, J. G., A. Opejin, A. Jones, C. Gross, and D. Hawiger. 2015. CD5 instructs extrathymic regulatory T cell development in response to self and tolerizing antigens. *Immunity* 42: 471–483.
26. McGuire, D. J., A. L. Rowse, H. Li, B. J. Peng, C. M. Sestero, K. S. Cashman, P. De Sarno, and C. Raman. 2014. CD5 enhances Th17-cell differentiation by regulating IFN-γ response and RORγt localization. *Eur. J. Immunol.* 44: 1137–1142.
27. Liebmann, M., S. Hucke, K. Koch, M. Eschborn, J. Ghelman, A. I. Chasan, S. Glander, M. Schädlich, M. Kuhlencord, N. M. Daber, et al. 2018. Nur77 serves as a molecular brake of the metabolic switch during T cell activation to restrict autoimmunity. *Proc. Natl. Acad. Sci. USA* 115: E8017–E8026.
28. Milam, A. A. V., J. M. Bartleson, D. L. Donermeyer, S. Horvath, V. Durai, S. Raju, H. Yu, V. Redmann, B. Zinselmeyer, J. M. White, et al. 2018. Tuning T cell signaling sensitivity alters the behavior of CD4+ T cells during an immune response. *J. Immunol.* 200: 3429–3437.
29. Weber, K. S., Q. J. Li, S. P. Persaud, J. D. Campbell, M. M. Davis, and P. M. Allen. 2012. Distinct CD4+ helper T cells involved in primary and secondary responses to infection. *Proc. Natl. Acad. Sci. USA* 109: 9511–9516.
30. Buck, M. D., D. O'Sullivan, and E. L. Pearce. 2015. T cell metabolism drives immunity. *J. Exp. Med.* 212: 1345–1360.
31. Buck, M. D., D. O'Sullivan, R. I. Klein Geltink, J. D. Curtis, C. H. Chang, D. E. Sanin, J. Qiu, O. Kretz, D. Braas, G. J. W. van der Windt, et al. 2016. Mitochondrial dynamics controls T cell fate through metabolic programming. *Cell* 166: 63–76.
32. Chang, C. H., J. Qiu, D. O'Sullivan, M. D. Buck, T. Noguchi, J. D. Curtis, Q. Chen, M. Gindin, M. M. Gubin, G. J. W. van der Windt, et al. 2015. Metabolic competition in the tumor microenvironment is a driver of cancer progression. *Cell* 162: 1229–1241.
33. O'Sullivan, D., G. J. W. van der Windt, S. C.-C. Huang, J. D. Curtis, C. H. Chang, M. D. Buck, J. Qiu, A. M. Smith, W. Y. Lam, L. M. DiPlato, et al. 2014. Memory CD8(+) T cells use cell-intrinsic lipolysis to support the metabolic programming necessary for development. [Published erratum appears in 2018 *Immunity* 49: 375–376.] *Immunity* 41: 75–88.
34. Sergushichev, A. A., A. A. Loboda, A. K. Jha, E. E. Vincent, E. M. Driggers, R. G. Jones, E. J. Pearce, and M. N. Artyomov. 2016. GAM: a web-service for integrated transcriptional and metabolic network analysis. *Nucleic Acids Res.* 44: W194–W200.
35. Ulland, T. K., W. M. Song, S. C.-C. Huang, J. D. Ulrich, A. Sergushichev, W. L. Beatty, A. A. Loboda, Y. Zhou, N. J. Cairns, A. Kambal, et al. 2017. TREM2 maintains microglial metabolic fitness in Alzheimer's disease. *Cell* 170: 649–663.e13.

36. Yadava, N., and D. G. Nicholls. 2007. Spare respiratory capacity rather than oxidative stress regulates glutamate excitotoxicity after partial respiratory inhibition of mitochondrial complex I with rotenone. *J. Neurosci.* 27: 7310–7317.
37. Kaye, J., M. L. Hsu, M. E. Sauron, S. C. Jameson, N. R. Gascoigne, and S. M. Hedrick. 1989. Selective development of CD4+ T cells in transgenic mice expressing a class II MHC-restricted antigen receptor. *Nature* 341: 746–749.
38. Lantz, O., I. Grandjean, P. Matzinger, and J. P. Di Santo. 2000. Gamma chain required for naïve CD4+ T cell survival but not for antigen proliferation. *Nat. Immunol.* 1: 54–58.
39. Zou, C., Y. Wang, and Z. Shen. 2005. 2-NBDG as a fluorescent indicator for direct glucose uptake measurement. *J. Biochem. Biophys. Methods* 64: 207–215.
40. Lo, W. L., D. L. Donermeyer, and P. M. Allen. 2012. A voltage-gated sodium channel is essential for the positive selection of CD4(+) T cells. *Nat. Immunol.* 13: 880–887.
41. Mráček, T., Z. Drahota, and J. Houštěk. 2013. The function and the role of the mitochondrial glycerol-3-phosphate dehydrogenase in mammalian tissues. *Biochim. Biophys. Acta* 1827: 401–410.
42. Langston, P. K., A. Nambu, J. Jung, M. Shibata, H. I. Aksoylar, J. Lei, P. Xu, M. T. Doan, H. Jiang, M. R. MacArthur, et al. 2019. Glycerol phosphate shuttle enzyme GPD2 regulates macrophage inflammatory responses. [Published erratum appears in 2019 *Nat. Immunol.* 20: 1555.] *Nat. Immunol.* 20: 1186–1195.
43. Liu, X., H. Qu, Y. Zheng, Q. Liao, L. Zhang, X. Liao, X. Xiong, Y. Wang, R. Zhang, H. Wang, et al. 2018. Mitochondrial glycerol 3-phosphate dehydrogenase promotes skeletal muscle regeneration. *EMBO Mol. Med.* 10: e9390.
44. Orr, A. L., D. Ashok, M. R. Sarantos, R. Ng, T. Shi, A. A. Gerencser, R. E. Hughes, and M. D. Brand. 2014. Novel inhibitors of mitochondrial sn-glycerol 3-phosphate dehydrogenase. *PLoS One* 9: e89938.
45. Klein, L., B. Kyewski, P. M. Allen, and K. A. Hogquist. 2014. Positive and negative selection of the T cell repertoire: what thymocytes see (and don't see). *Nat. Rev. Immunol.* 14: 377–391.
46. Myers, D. R., E. Norlin, Y. Vercoulen, and J. P. Roose. 2019. Active tonic mTORC1 signals shape baseline translation in naive T cells. *Cell Rep.* 27: 1858–1874.e6.
47. Zheng, Y., G. M. Delgoffe, C. F. Meyer, W. Chan, and J. D. Powell. 2009. Anergic T cells are metabolically anergic. *J. Immunol.* 183: 6095–6101.
48. Bailis, W., J. A. Shyer, J. Zhao, J. C. G. Canaveras, F. J. Al Khazal, R. Qu, H. R. Steach, P. Bielecki, O. Khan, R. Jackson, et al. 2019. Distinct modes of mitochondrial metabolism uncouple T cell differentiation and function. [Published erratum appears in 2019 *Nature* 573: E2.] *Nature* 571: 403–407.
49. Ma, E. H., M. J. Verway, R. M. Johnson, D. G. Roy, M. Steadman, S. Hayes, K. S. Williams, R. D. Sheldon, B. Samborska, P. A. Kosinski, et al. 2019. Metabolic profiling using stable isotope tracing reveals distinct patterns of glucose utilization by physiologically activated CD8+ T cells. *Immunity* 51: 856–870.e5.
50. Wolf, T., W. Jin, G. Zoppi, I. A. Vogel, M. Akhmedov, C. K. E. Bleck, T. Beltraminelli, J. C. Rieckmann, N. J. Ramirez, M. Benevento, et al. 2020. Dynamics in protein translation sustaining T cell preparedness. *Nat. Immunol.* 21: 927–937.